Corrections to "Photonic Sub-Terahertz IM Links: Comparison Between Double and Single Carrier Modulation"

Luis Gonzalez-Guerrero, Muhsin Ali, Robinson Guzman, Horacio Lamela, and Guillermo Carpintero, *Senior Member, IEEE*

***Abstract*—In this manuscript we report four mistakes in [1] and their respective corrections. Two mistakes are notation typos with no implications, whereas the other two are mistakes regarding the simulations. The correction of these two mistakes changes slightly the technical analysis presented in [1], however, they do not affect the main conclusions reported in such a paper.**

***Index Terms*—Amplitude modulation, communication systems, microwave photonics, optoelectronic devices, sub-THz communication.**

I. Comments and Corrections

WE FOUND four mistakes in [1], which are now discussed through bullet points in the order of appearance in [1]. Apart from these mistakes, we also make some comments for the sake of a better understanding of [1].

Correction I: in Section II-B of [1], $\langle I_{THz}^2 \rangle$ in the D-C scheme should be equal to $2(P_0^2 + m^2\, s^2(t))$ and not to $2P_0^2 + m^2\, s^2(t)$. The former expression was used in [1], and thus, the analysis and results presented in that section remain unchanged.

Comment I: the simulation diagram in [1] (i.e., Fig. 4 of [1]) is incomplete as it only provides information about the simulation structure used for the D-C scheme. Fig. 1 in this manuscript provides a more accurate structure of the simulations. As can be seen, for the S-C scheme, the photodiode (PD) block is just a multiplication by one. This is because, in this scheme, the PD performs an heterodyne beating between an unmodulated tone and the data signal. This results in only a change in the data signal carrier frequency but not in its baseband waveform. In the the D-C scheme, on the other hand, two data signals are beaten together, leading to the square operation shown in the D-C diagram in Fig. 1 of this manuscript.

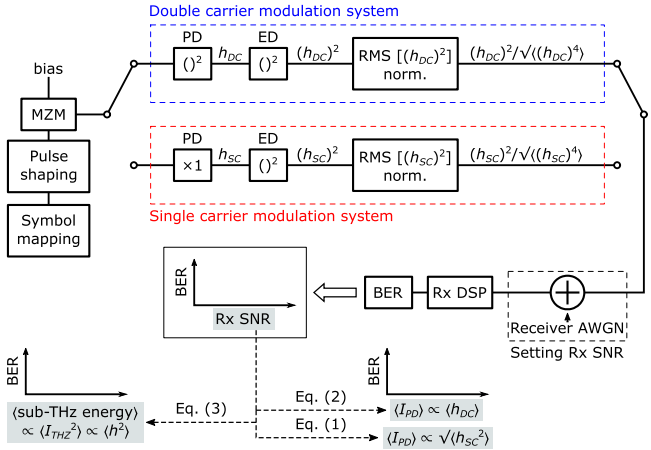

Fig. 1. Structure of the simulations used in [1] and in this manuscript (in the results discussed in Correction IV, Comment VI, and Comment VII). The diagram also shows the equations employed to calculate $\langle I_{PD} \rangle$ and $\langle I_{THz}^2 \rangle$ from receiver SNR.

Comment II: in [1] we also did not justified what type of noise is considered in the simulations and why it is added after the envelope detector (ED) block. The noise used in the simulations in [1] is additive white Gaussian noise (AWGN) and it is added after the PD as thermal receiver noise is assumed to dominate over any other noise source. This is typically the case for sub-THz systems where transmitter noise is attenuated by the high free-space path loss found at these frequencies and mixer down conversion loss [2], [3].

Comment III: in [1], we employ the term "normalization factor" to refer to the independent variable against which the bit error ratio (BER) is measured. Four such independent variables are discussed in [1]: signal-to-noise ratio (SNR), average photocurrent, average sub-THz energy, and average optical power from the lasers. Using the term "normalization factor" to refer to such variables might not be appropriate terminology – a better term could be "characterization variable". However, for the sake of readability and easy understanding, the same terminology as in [1] is used in this manuscript.

Comment IV: in Section II of [1] we discuss three normalization factors: average photocurrent ($\langle I_{PD} \rangle$), average sub-THz

Manuscript received 13 January 2023; accepted 24 February 2023. Date of publication 30 March 2023; date of current version 16 May 2023. This work was supported in part by the European Commission and UC3M through the Marie-Sklodowska Curie COFUND Action under Grant H2020-MSCA-COFUND-2017 GA 801538, in part by the Spanish Ministerio de Ciencia e Innovaci'on through Programa Estatal de Generaci'on de Conocimiento y Fortalecimiento Cientfico y Tecnolgico del sistema de I+D+i orientada a los Retos de la Sociedad convocatoria 2019 under Grant PID2019-109984RB-C42, and in part by the European Union through the Horizon 2020 Research and Innovation Programme under Grant 871668 (TERAWAY Project, which is an initiative of the Photonics Public Private Partnership). *(Corresponding author: Luis Gonzalez-Guerrero.)*

The authors are with the Grupo de Optoelectronica y Tecnologia Laser (GOTL), Universidad Carlos III de Madrid, 28911 Madrid, Spain (e-mail: lgguerre@ing.uc3m.es; muali@ing.uc3m.es; rcguzman@ing.uc3m.es; horacio@ing.uc3m.es; guiller@ing.uc3m.es).

Color versions of one or more figures in this article are available at https://doi.org/10.1109/JLT.2023.3254301.

Digital Object Identifier 10.1109/JLT.2023.3254301

energy, and average optical power from the lasers. On the other hand, in Section III of [1], the BER is measured against $\langle I_{PD}\rangle$ and SNR. It is important to clarify that SNR in [1] refers to receiver SNR and that it is a different normalization factor from the average sub-THz energy factor we discuss in Section II-B of [1] (which is proportional to $\langle I_{THz}^2\rangle$ and it is related to receiver SNR by a quadratic operation).

Whereas receiver SNR is used in the simulations, this normalization factor is missing in the analysis of Section II in [1]. We now provide an analytical discussion of the performance of each scheme under SNR normalization. Receiver SNR is proportional to $\langle I_{ED}^2\rangle$, which is easy to show (remembering that $m^2\, s^2(t) = P_0^2$ when the signal is an ideal rectangular pulse) that is equal to $32P_0^4$ and to $8P_0^4$ for the D-C and S-C cases, respectively. To normalize both schemes for an equal value of $\langle I_{ED}^2\rangle$ – for example, $\langle I_{ED}^2\rangle = 32P_0^4$ – the ED signal (i.e., I_{ED}) in the S-C scheme has to be multiplied by $\sqrt{4} = 2$. This means multiplying V_{pSC} also by two giving a peak voltage in the recovered signal of $4P_0$, which is the peak voltage of the recovered signal in the D-C scheme for $\langle I_{ED}^2\rangle = 32P_0^4$. Hence, for receiver-SNR normalization both schemes should exhibit the same performance.

Correction II: in both (17) and (18) in [1], the denominator should be the forth root of the *average* of the S-C and D-C waveforms to the power of four so that (17) should be:

$$\langle I_{PD}\rangle \propto \frac{\sqrt[4]{SNR}\cdot\sqrt{\langle h_{SC}^2(t)\rangle}}{\sqrt[4]{\langle h_{SC}^4(t)\rangle}}, \tag{1}$$

and (18) should be:

$$\langle I_{PD}\rangle \propto \frac{\sqrt[4]{SNR}\cdot\langle h_{DC}(t)\rangle}{\sqrt[4]{\langle h_{DC}^4(t)\rangle}}. \tag{2}$$

The expressions provided in this manuscript were used in [1], and, thus, the results are not affected.

Comment V: as shown in Fig. 1 of this manuscript, in the simulations, the BER is calculated for specific values of receiver SNR. To compute the BER-vs-$\langle I_{PD}\rangle$ curves shown in Fig. 5 of [1], receiver SNR values are converted to a quantity proportional to $\langle I_{PD}\rangle$ by means of (1) and (2) in this manuscript for the S-C and D-C schemes respectively. Unlike SNR values, which are absolute, $\langle I_{PD}\rangle$ values are relative, since specific values depend on several factors such as transmission distance, PD responsivity, etc., and that is why $\langle I_{PD}\rangle$ values in Fig. 5 of [1] are arbitrary. We note, however, that the relative $\langle I_{PD}\rangle$ penalty between schemes (i.e., the ratio between the $\langle I_{PD}\rangle$ values required by each scheme to achieve a certain BER) is absolute.

Correction III: in Section III-A we compare the simulation results obtained for receiver SNR normalization and 2-PAM signalling to those derived in Section II-B. This is wrong, as in Section II-B the normalization factor being discussed is average sub-THz energy (i.e., $\langle I_{THz}^2\rangle$), which, as mentioned in Comment IV of this manuscript, is different from receiver SNR. To properly compare the results of the simulations with the mathematical analysis given in Section II-B of [1], in this manuscript we also provide the BER-vs-$\langle I_{THz}^2\rangle$ curves for both the S-C and D-C schemes (such a curves are discussed in Correction IV, Comment VII, and Comment VIII). As happens with $\langle I_{PD}\rangle$ values, $\langle I_{THz}^2\rangle$ values are also relative since absolute values depend on system specifications. However, the $\langle I_{THz}^2\rangle$ penalty between the two schemes should be absolute. To calculate $\langle I_{THz}^2\rangle$ values from receiver SNR ones, the following equation needs to be used:

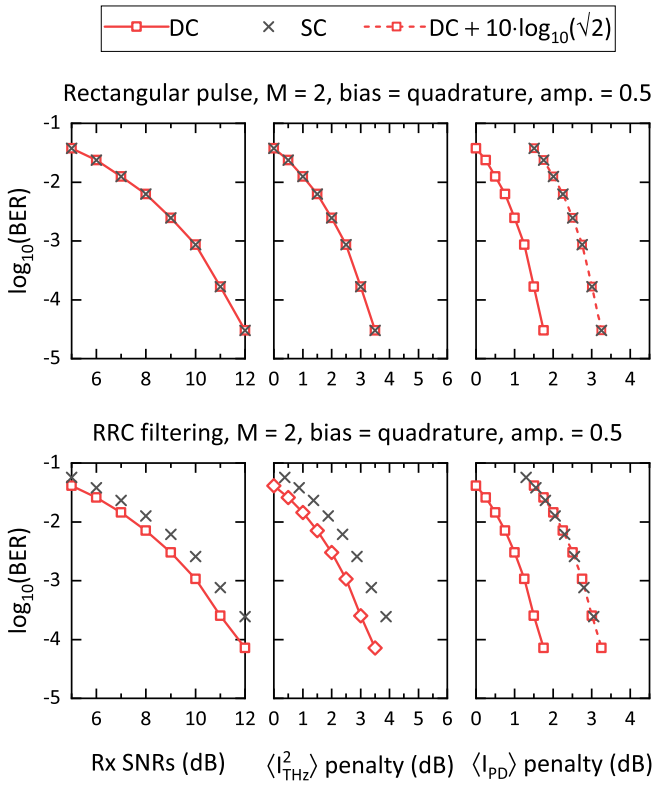

Fig. 2. BER curves obtained for biasing of the MZM in the quadrature point, 2-PAM, a normalized amplitude of 0.5, and rectangular pulse shaping (first row) and RRC filtering (second row).

$$\langle I_{THz}^2\rangle \propto \frac{\sqrt[2]{SNR}\cdot\langle h^2(t)\rangle}{\sqrt[2]{\langle h^4(t)\rangle}}, \tag{3}$$

where $h(t)$ refers to $h_{SC}(t)$ and $h_{DC}(t)$ for the S-C and D-C schemes, respectively.

Comment VI: the only normalization factor that is not included in the simulations of this manuscript is the average optical power from the lasers. This is because, as shown in Table I of [1], the penalty between schemes under this factor is dependent on modulator loss, which can take a wide range of values according to manufacturer and model. In any case, we remind the reader, that, when a MZM is used for IM (i.e., at the quadrature point), a MZM insertion loss higher than 0 dB will cause the S-C scheme to outperform the D-C scheme even under 2-PAM.

Correction IV: in the analysis of Section II of [1], we consider rectangular pulse shaping and ideal IM. However, in the simulations of [1], an RRC filter is used for pulse shaping and the bias of the MZM is not fixed at quadrature, which is the point required for IM. This make the simulation results deviate from the mathematical analysis of [1] and it is the reason why there is some penalty between the S-C and D-C$\times\sqrt{2}$ curves in Fig. 5(b) of [1]. In Fig. 2 of this manuscript, we show the results of the

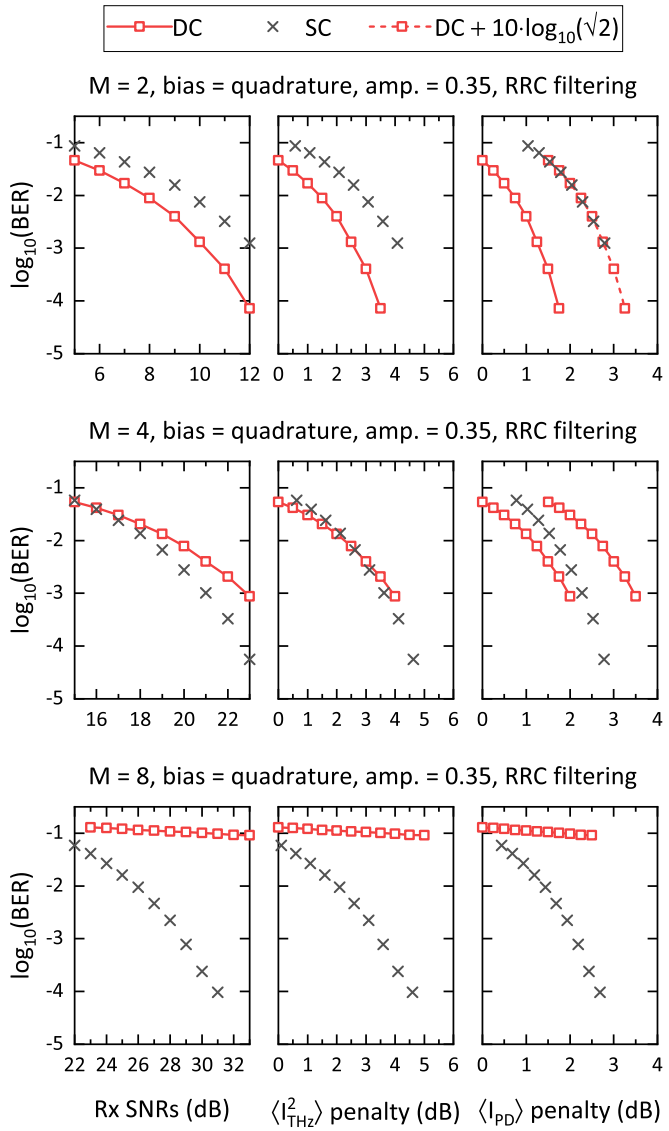

Fig. 3. BER curves obtained for biasing of the MZM in the quadrature point, a normalized amplitude of 0.35, RRC filtering, and M = 2 (first row), M = 4 (second row) and M = 8 (third row).

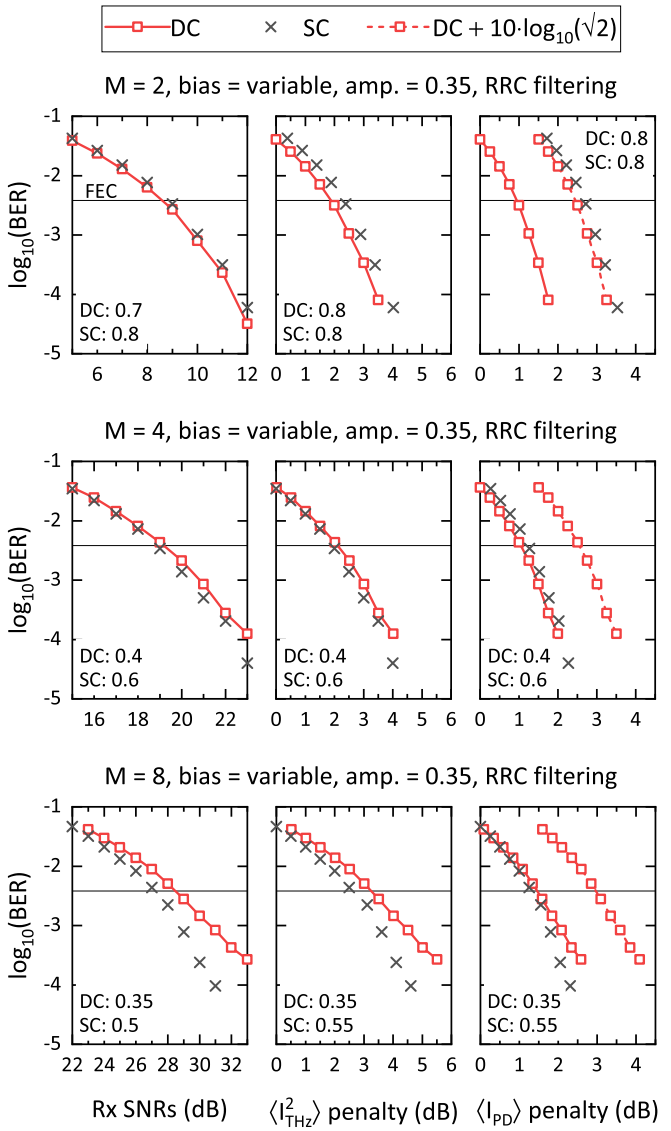

Fig. 4. BER curves obtained for the optimum MZM biasing point, a normalized amplitude of 0.35, RRC filtering, and M = 2 (first row), M = 4 (second row) and M = 8 (third row).

simulations when the MZM bias is set at quadrature. The first row of graphs in Fig. 2 corresponds to rectangular pulse shaping, whereas the second row is for RRC shaping (both for 2-PAM signalling). In the two cases, a normalized modulation amplitude of 0.5 is used (unlike in [1], where the amplitude is set to 0.35). The reason to use this value (which corresponds to a peak voltage in the modulating signal equal to the modulator π-voltage) is that an infinite ER is assumed in the comparison given in Section II-B in [1] and a normalized modulation amplitude of 0.5 is the value required to achieve such an ER when the MZM is biased at quadrature.

In this manuscript, the units of $\langle I_{PD}\rangle$, as well as those of $\langle I^2_{THz}\rangle$, are given in dB instead of linear units to emphasize the fact that the units are relative and not absolute. Both $\langle I_{PD}\rangle$ and $\langle I^2_{THz}\rangle$ values are referenced to the lowest $\langle I_{PD}\rangle$ and $\langle I^2_{THz}\rangle$ values that appear in each plot.

As can be seen, when the MZM is biased at quadrature, the normalized amplitude is 0.5, and the pulse shaping is rectangular, the results of the simulations agree perfectly with the analysis in Sections II-A and II-B, which predict that the S-C and D-C schemes have a penalty of $\sqrt{2}$ under $\langle I_{PD}\rangle$ normalization but that should have the same performance under $\langle I^2_{THz}\rangle$ normalization. Note that, in this case, the nonlinear nature of the MZM is irrelevant because the electrical signal only takes two discrete levels and ideal optical IM is achieved. It can also be seen that both schemes have the same performance under SNR normalization as predicted in Comment IV of this manuscript.

When RRC filtering is employed, the electrical signal is not binary any more and the nonlinearity of the MZM prevents the generation of ideal IM. In spite of this, the same $\sqrt{2}$ penalty is found between the two schemes under $\langle I_{PD}\rangle$ normalization and a very similar performance is obtained under both $\langle I^2_{THz}\rangle$ and

receiver SNR normalization (penalty less than 1 dB between the two schemes).

Comment VII: to see the penalty between the two schemes for different modulation orders under IM, in Fig. 3 of this manuscript we show the BER results for M = 2, 4, and 8 (i.e., 2-PAM, 4-PAM, and 8-PAM) when the MZM is biased at quadrature (this is unlike Fig. 5 in [1], where the BER curves are obtained for the optimum biasing of the MZM). To avoid strong nonlinear distortions in the higher order formats, the normalized amplitude is lowered to 0.35. As can be seen from Fig. 3, the penalty of the S-C scheme under all three normalization factors progressively vanishes as the modulation order increases. This is consistent with our hypothesis in [1] about the SSBI being the cause of the D-C performance degradation as the modulation order is increased.

Comment VIII: finally, in Fig. 4 of this manuscript we show a modified version of Fig. 5 in [1]. Compared to such a figure, here: a) we show the BER results also under $\langle I_{THz}^2 \rangle$ normalization, b) the x-axis units are all in dB, and c) we include (in the legend inside each figure) the optimum biasing point at the 7% FEC limit (i.e., BER of 3.8×10^{-3}). The optimum biasing point is included to show how signals that are less affected by SSBI (i.e., the S-C scheme) have higher optimum biasing points than those with higher SSBI (i.e., the D-C scheme).

REFERENCES

[1] L. Gonzalez-Guerrero, M. Ali, R. Guzman, H. Lamela, and G. Carpintero, "Photonic sub-terahertz IM links: Comparison between double and single carrier modulation," *J. Lightw. Technol.*, vol. 40, no. 18, pp. 6064–6070, Sep. 2022.

[2] A. J. Seeds, H. Shams, M. J. Fice, and C. C. Renaud, "TeraHertz photonics for wireless communications," *J. Lightw. Technol.*, vol. 33, no. 3, pp. 579–587, 2015.

[3] R. Piesiewicz et al., "Short-range ultra-broadband terahertz communications: Concepts and perspectives," *IEEE Antennas Propag. Mag.*, vol. 49, no. 6, pp. 24–39, Dec. 2007.